NIST Technical Note
NIST TN 2294

Test Facility for Pressure Losses in Plumbing Pipes and Fittings

Lingnan Lin
Natascha Milesi Ferretti
Glen Glaeser

This publication is available free of charge from:
https://doi.org/10.6028/NIST.TN.2294

NIST NATIONAL INSTITUTE OF STANDARDS AND TECHNOLOGY
U.S. DEPARTMENT OF COMMERCE

NIST Technical Note
NIST TN 2294

Test Facility for Pressure Losses in Plumbing Pipes and Fittings

Lingnan Lin
Natascha Milesi Ferretti
Glen Glaeser
Building Energy and Environment Division
Engineering Laboratory

This publication is available free of charge from:
https://doi.org/10.6028/NIST.TN.2294

July 2024

U.S. Department of Commerce
Gina M. Raimondo, Secretary

National Institute of Standards and Technology
Laurie E. Locascio, NIST Director and Under Secretary of Commerce for Standards and Technology

NIST TN 2294
July 2024

Publication History
Approved by the NIST Editorial Review Board on 2024-07-05

How to Cite this NIST Technical Series Publication
Lin L, Milesi-Ferretti N, Glaeser G (2024) Test Facility for Pressure Losses in Plumbing Pipes and Fittings. (National Institute of Standards and Technology, Gaithersburg, MD), NIST Technical Note (TN) NIST TN 2294. https://doi.org/10.6028/NIST.TN.2294

NIST Author ORCID iDs
Lingnan Lin: 0000-0002-0813-7613
Natascha Milesi Ferretti: 0009-0007-7273-0925
Glen Glaeser: 0009-0007-9383-5224

Contact Information
natascha.milesi-ferretti@nist.gov

Abstract

This report describes a new test facility at NIST for the measurement of pressure losses in pipes and fittings used in plumbing systems for water supply and distribution. Pressure losses are fundamental inputs to the design of premise plumbing systems, yet the available technical data on pressure loss in pipe fittings are limited and largely outdated. The Plumbing Hydraulics Laboratory is designed to test plumbing pipes, tubing, and fittings of different materials and different types, including couplings, reducers/expanders, elbows, tees, and crosses, for Nominal Tube Size (NTS) from ½ to 1. The laboratory is designed to operate at velocities between 0.3 m/s and 4.6 m/s (1.0 ft/s and 15 ft/s) in the test section. The static pressure at different locations along the test section is measured using custom-made piezometer rings, an array of differential pressure transducers of different ranges, and an automatic pressure switching system. The measured pressure distribution can be used to derive the friction factor of a straight pipe and the pressure loss coefficient of a fitting. Several tests have been carried out for a straight pipe (NTS ¾, Type L, copper) to validate the method and the instrumentation. The measured friction factors show excellent repeatability and are within ± 3 % of the Colebrook correlation. The test facility will be used to generate benchmark pressure loss data for modern plumbing pipes and fittings and to improve the understanding of the flow characteristics in modern fittings. Through research activities in this test facility, we aim to facilitate the development of a simple, accurate, and cost-effective test method that can be implemented in the plumbing industry as well as other piping applications (e.g., hydronic heating and cooling, fire protection).

Keywords

Pressure, Flow, Water, Fittings, Pipes, Plumbing.

Table of Contents

List of Tables

List of Figures

Acknowledgments

The authors gratefully acknowledge Marylia Duarte-Batista for her critical contributions to the original design of the Plumbing Hydraulics Laboratory, NIST Technicians Luis Luyo and Tyler Gervasio for their support in constructing the test rig, Lance MacNevin of the Plastic Pipe Institute for helpful discussions and publication review, Dr. John Wright formerly of the NIST Fluid Metrology Group for valuable discussions on instrumentation for flow and pressure measurements, Gary Klein of Gary Klein and Associates for sharing his insights on measurement challenges in premise plumbing, and Emily Liu and Braedon Mullin of the University of Maryland for their analytical and experimental works during their summer internships.

1. Introduction

Premise plumbing systems provide reliable access to clean water and sanitation, which is an essential building service. Modern plumbing designs aim to optimize water usage through technology and water management while considering functional requirements, system capacity, system and material limitations, applicable plumbing codes, and industry standards. However, incorrect pipe sizing in hot- and cold-water distribution systems can impede achieving design flows, increase operating and installed cost, reduce energy efficiency, and increase the building's carbon footprint. Incorrect pipe sizing can also result in reduced flow rates that can contribute to water stagnation, decay of disinfectants, potential growth of biofilms and opportunistic pathogens, and reduced water quality. Therefore, the pressure losses within piping systems are of primary importance to the sizing of pipes, fittings, and pumps.

Since the original plumbing codes of the 1920s (i.e., the Hoover Codes [1]), there have been significant technological advances in product design, including advances that promote water efficiency and water quality and a significant shift in the materials of construction and joining methods used for both pipes and fittings. However, some original data and calculations in the Hoover Codes are still being used today for plumbing design. This is problematic as the data are not representative of modern fittings and flow conditions. The current water use in buildings, on a per-fixture basis, is much lower than that in the 20th century due to control advances such as improved aeration and automatic shut-off, and the peak water use is much lower than what building codes require. Also, there has been a fundamental shift in materials and design concepts that are implemented in modern buildings, including the predominant use of copper and plastics as the material of construction, and the use of innovative water distribution designs to reduce dead ends and unnecessarily long runs. The National Institute of Building Sciences (NIBS)'s Consultative Council recently published a report [2] that highlights the link between plumbing design and decarbonization, noting "right-sizing of plumbing systems in residential occupancies and an overall reduction of pipe sizes in the built environment… not only leads to improved water efficiency, but also an overall reduction in carbon footprint in the built environment of plumbing systems."

For modern premise plumbing systems to meet the performance goals of protecting occupant health, increasing efficiency, and reducing environmental impacts, an entirely new technical knowledge base must be developed. In its 2016 annual report [3], the NIBS Consultative Council identified several measurement science needs related to premise plumbing, specifically calling on NIST to resume premise plumbing research to modernize water pipe-sizing calculations.

Regardless of whether designers use the equivalent length method or the excess head method, the pressure loss in plumbing systems is fundamental to sizing water distribution pipes. One of the current shortcomings of these methods is that the pressure loss is often estimated. Lin et al. [4] reviewed the existing data, published from 1926 to 2021, on pressure loss of fluid flow through pipe fittings. The literature review confirmed that most of the existing data are not representative of modern pipe fittings. A large portion of data are pre-1950s and based on malleable iron and wrought steel fittings. There is also very limited data for copper, PVC, CPVC and PEX fittings, particularly for diameters at or less than 1 inch (25.4 mm). Figure 1 shows the

digitized data for pressure loss in elbows. It is evident that pressure loss data for elbows show a large variation across the data.

Other identified gaps include [5]: 1) no standard test method for pressure loss in fittings, 2) measured data not widely available for specific fittings and configurations, and 3) reported pressure loss of fittings often estimated from literature values that may not be accurate. In 2021, NIST began to design and build a test facility to measure the pressure loss in plumbing fittings and facilitate the development of standard test methods.

This report documents the measurement principles to accurately quantify pressure losses in pipes and fittings, provides a description of the NIST Plumbing Hydraulics Laboratory, and discusses the instrumentation and measurement techniques employed along with the reasoning for their selection. It is intended that this unique test facility provide updated technical data on the pressure loss in pipe fittings to support the modernization of design and operation.

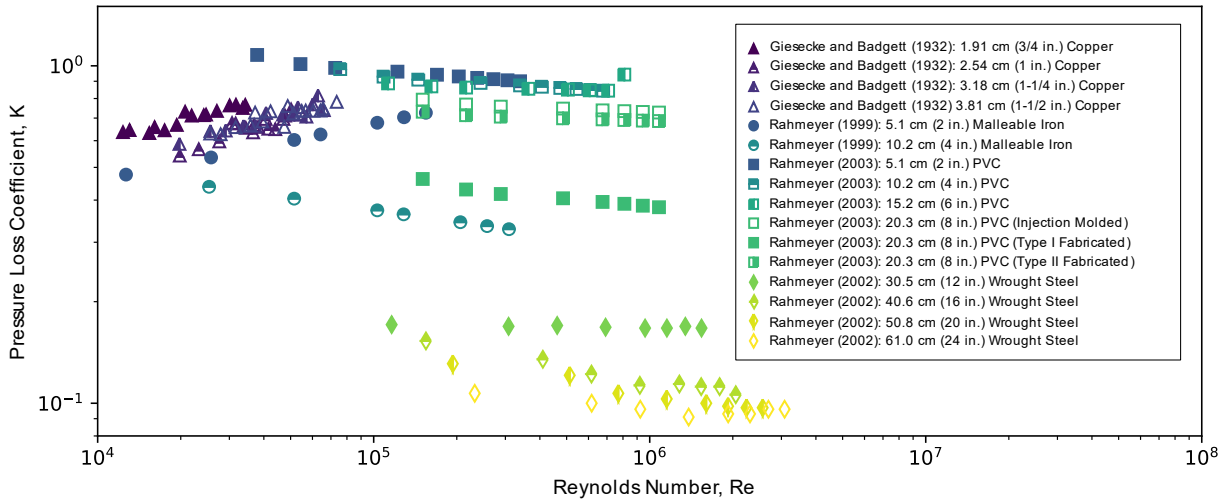

Figure 1. Existing data for elbows (data source: Giesecke and Badgett (1932) [6]; Rahmeyer (1999) [7]; Rahmeyer (2002) [8]; Rahmeyer (2003) [9]).

2. Measurement Principles

Pressure loss is an irreversible loss of mechanical energy of a flowing fluid. Pressure losses caused by pipes and fittings are referred to as “major loss” and “minor loss”, respectively, in most textbooks and engineering handbooks. While pressure losses in pipes are caused by the fluid friction, pressure losses in fittings are primarily due to the flow separation and mixing effects induced by a change of flow direction or cross section [4]. The term “pressure drop” is sometimes used alternatively or interchangeably with “pressure loss” in industry and other communications. However, they are not equivalent. A “pressure drop” is simply the reduction of the static pressure. It includes not only friction and other irreversibilities, but also acceleration (e.g., flow through a reducer) or elevation. In plumbing design, the pressure change due to the change of pipe size and/or elevation is generally calculated separately, and hence it should not be included again when evaluating fittings. Therefore, the term “pressure loss” is recommended and used in this report as well as by the NIST Plumbing Hydraulics Lab.

Pressure losses in pipes and fittings can be accurately determined by establishing the pressure distribution, or the “hydraulic grade line”, which can be obtained by measuring the static pressure at several different locations along the pipe. Figure 2 illustrates a hydraulic grade line of a fluid flowing through straight pipes connected by a fitting.

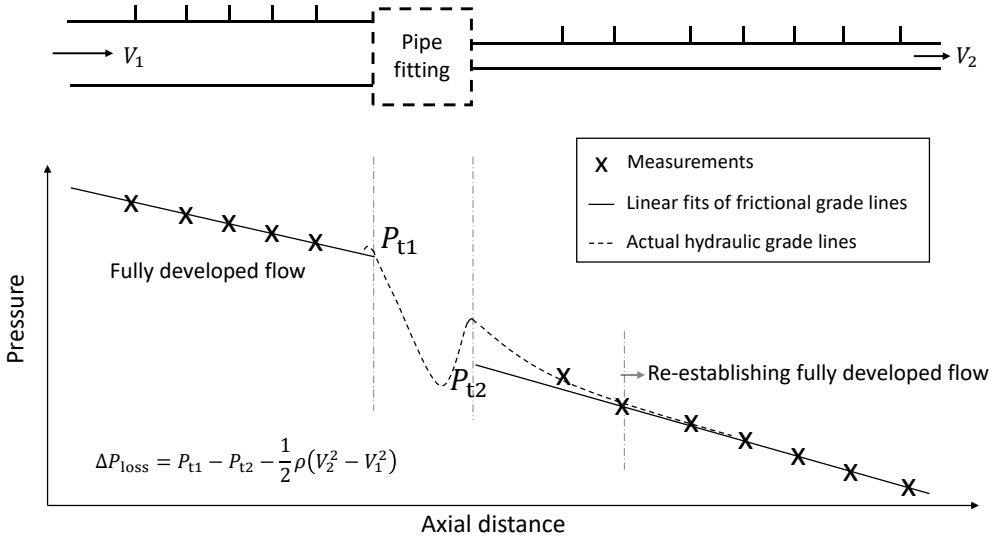

Figure 2. Illustration of a hydraulic grade line.

The pressure loss of a fully-developed flow in straight pipes is linear and can be described by the Darcy–Weisbach equation:

$$\Delta P_{L,\mathrm{fr}} = f\frac{\Delta L}{D}\frac{\rho V^2}{2} \tag{1}$$

wherein,

ΔP - Pressure difference
f - Friction factor
ΔL - Length
D - Pipe diameter
ρ - Density
V - Average velocity

The presence of a fitting causes a pressure loss and a diversion in the hydraulic grade line, which occurs not only within the fitting, but also slightly upstream and significantly downstream. The impact wanes as the flow fully redevelops and the linear relationship is again established.

The pressure loss due to the fitting ($\Delta P_{L,\mathrm{t}}$) can be calculated by:

$$\Delta P_{L,\mathrm{t}} = P_{t1} - P_{t2} \tag{2}$$

where P_{t1} is the value of the hydraulic grade line extended from the upstream fully-developed region to the fitting inlet, P_{t2} is the value of the hydraulic grade line extended from the downstream fully-developed region to the fitting outlet.

In cases of reducer and expansion fittings, the effect of acceleration or deceleration due to the change of diameter must be considered, and Eq. (2) becomes:

$$\Delta P_{L,\mathrm{t}} = P_{t1} - P_{t2} + \frac{1}{2}\rho(V_1^2 - V_2^2) \tag{3}$$

Eq. (3) also applies to branching fittings such as tees and crosses. In this case, the hydraulic grade line is, with respect to the flow, to or from a specific branch, as is the computed pressure loss of the fitting.

The measured pressure loss may be reduced to loss coefficient, K_L, to characterize a given pipe fitting:

$$K_L = \frac{\Delta P_{L,\mathrm{t}}}{\rho V^2/2} \tag{4}$$

3. Test Facility

The test facility is designed to measure the pressure loss for various fittings (i.e., various types, materials, and diameters) over a range of flow velocity from 0.3 m/s to 4.6 m/s (1.0 ft/s to 15 ft/s). Figure 3 shows the schematic of the test facility. It is a recirculation system of water driven by a centrifugal pump. The pump draws water from the bottom of a 190 L (50 gal.) tank to the test section, where the pressure loss of a fitting sample is measured, and then the water is returned to the tank. The water level in the tank is maintained at approximately 3.7 m above the pump to provide sufficient net positive suction head (NPSH) and prevent cavitation. The entire facility is approximately 4.6 m long, 2.4 m wide, and 2.1 m high. The facility size is limited by the lab space, and this limits the length of the test section and thereby the diameter of test pipes and fittings (up to 2.54 cm or 1 in.).

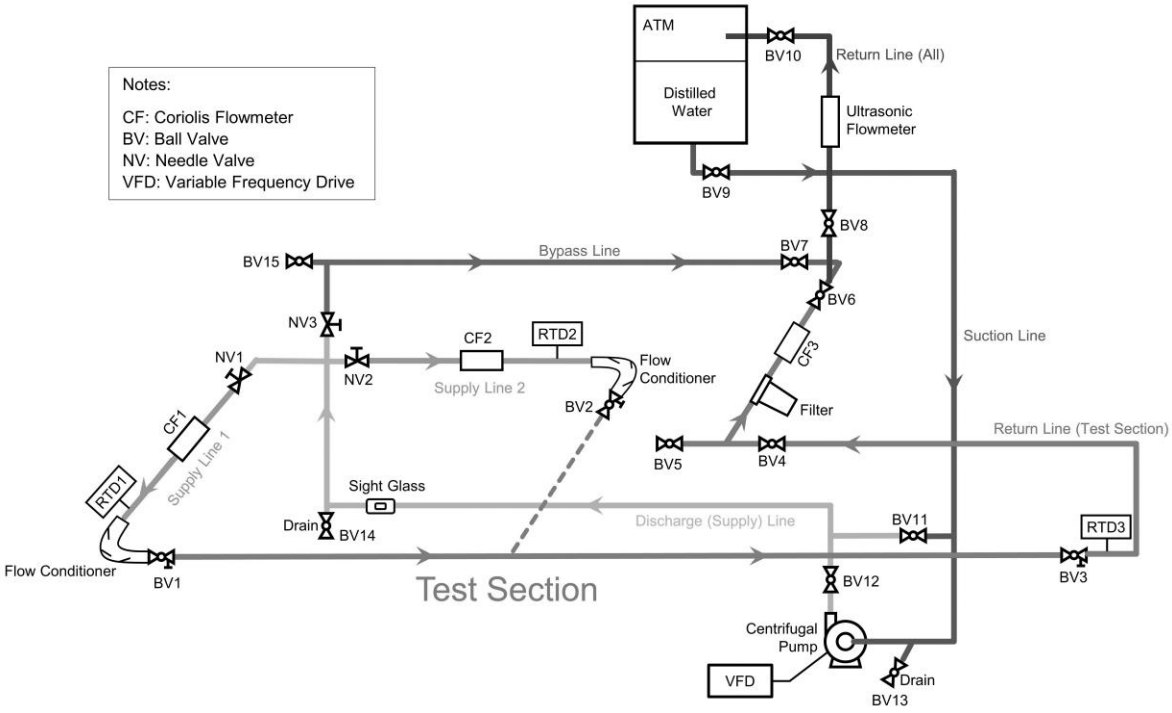

Figure 3. Schematic of the test facility.

The test section is approximately 3.7 m (12 ft.) long, constructed on a horizontal plane 1.8 m (6.0 ft.) above the ground. There are two supply lines branched from the pump discharge line to the inlet(s) of the test section. The two supply lines are identical in length and instrumentation, and they are connected at a 90° angle, which allows different piping configurations of the test section for different types of fittings, as shown in Figure 4. The test section consists of a test fitting and two to four straight pipes connected by the fitting, depending on the type of the fitting. For two-way fittings (i.e., flow-through fittings), the lengths of upstream and downstream pipes are 1.5 m (5.0 ft.) and 2.1 m (7.0 ft.), respectively. The same upstream pipe can be used for testing straight fittings (e.g., straight coupler or reducer/expander) and elbows. The switch can be done by disconnecting the upstream pipe from Supply Line 1 and connecting it to Supply Line 2. For three-way fittings (i.e., tees), an additional upstream pipe is used, and

the flow can be from either one of Supply Lines 1 and 2, or from both of them with different flow ratios. Four-way fittings (i.e., cross) can also be tested by connecting additional pipes or hoses to the valve BV5. Push-to-connect fittings are used to connect test section pipes and supply and return lines, allowing simple and quick installation and modification of test section. All pipes in the test section have multiple pressure taps for measurement of pressure distribution (see Sec. 4.1).

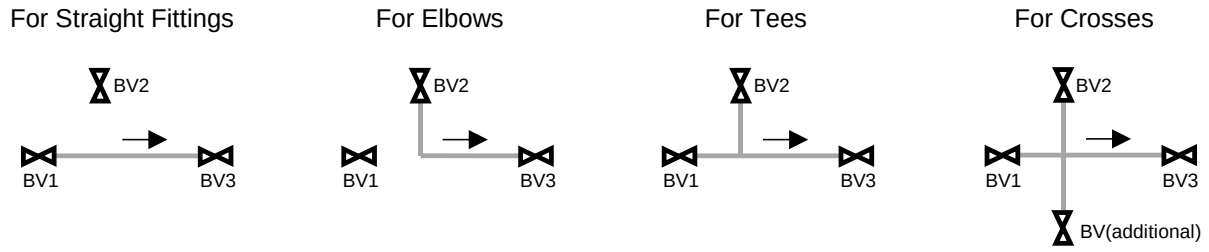

Figure 4. Test section configurations for different fitting types.

A flow conditioning elbow is installed before each inlet of the test section to reduce the straight run needed to establish fully developed flow. As shown in Figure 5, the flow conditioning elbow features tabs along the outer wall that can reduce swirl and correct the velocity profile. This design helps the exiting flow quickly develop a symmetric velocity profile, which is important for repeatability and accuracy of the pressure measurement in the test section. Detailed specifications of the flow conditioning elbow are given in Appendix A.1.

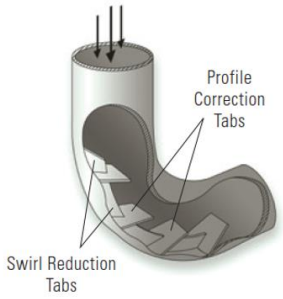

Figure 5. Flow conditioning elbow (from [10])

The pump is sized to provide a velocity up to 4.6 m/s (15 ft/s) in the test section. Since the largest test pipe is NTS 1 (approximately 25.4 mm OD), the maximal designed flow rate is then 2.31 kg/s (36.7 gpm). A centrifugal pump is chosen because it can provide high flow rate with relatively small pulsation and fluctuation. The centrifugal pump used has a 316 L stainless steel impeller with diameter of 155.6 mm (6-1/8 in.). The suction and discharge ports are NTS 1-1/4 and NTS 1, respectively. Detailed specifications of the pump are given in Appendix A.2.

A variable frequency drive (VFD) is used to control the pump speed to control the flowrate. When the pump reaches its minimum speed, lower flowrates are achieved by adjusting the needle valves in the Supply Line 1 or 2. The pump minimum speed is established to ensure adequate cooling for the pump motor, thereby extending its service life. For real-time control, the VFD communicates with the lab computer through two (4 to 20) mA inputs, two (4 to 20)

mA outputs, and a Fieldbus communication module. Detailed specifications of the VFD are given in Appendix A.3.

The test rig is plumbed by NTS 1 copper pipes, except that NTS 1-1/4 copper pipe is used for the suction line that connects the centrifugal pump and the water tank. Vibration-damping clamps are used to mount the pipes onto aluminum supporting frames to minimize the impact of the pump vibration on the flow.

4. Instrumentation and Measurement Techniques

4.1. Pressure Measurements

The pressure measurement system consists of pressure taps, piezometer rings, differential pressure sensors, an absolute pressure transducer, an automatic switching system, and an in-situ calibration system. The schematic and photo of the system are shown in Figure 6 and Figure 7, respectively. Most components of the pressure measurement system are mounted on an aluminum plate that is 1.2 m by 0.9 m by 4.7 mm (i.e., 46 in. by 36 in. by 3/16 in.) and supported by aluminum frames. These aluminum frames are intentionally disconnected from any frame supporting pipes to eliminate the impact of pump-induced vibration on the pressure measurement. The instrumentation and measurement techniques associated with the pressure measurement components are described as follows.

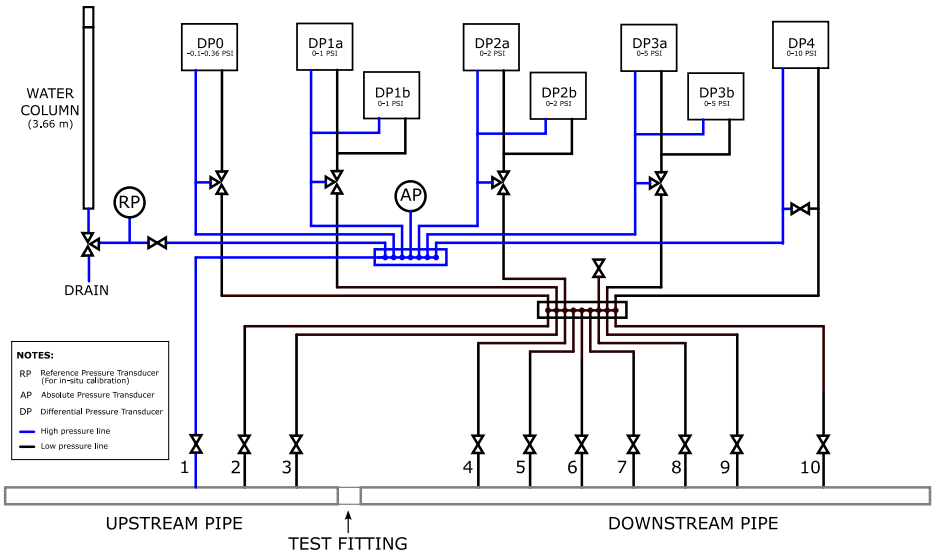

Figure 6. Schematic of the pressure measurement system.

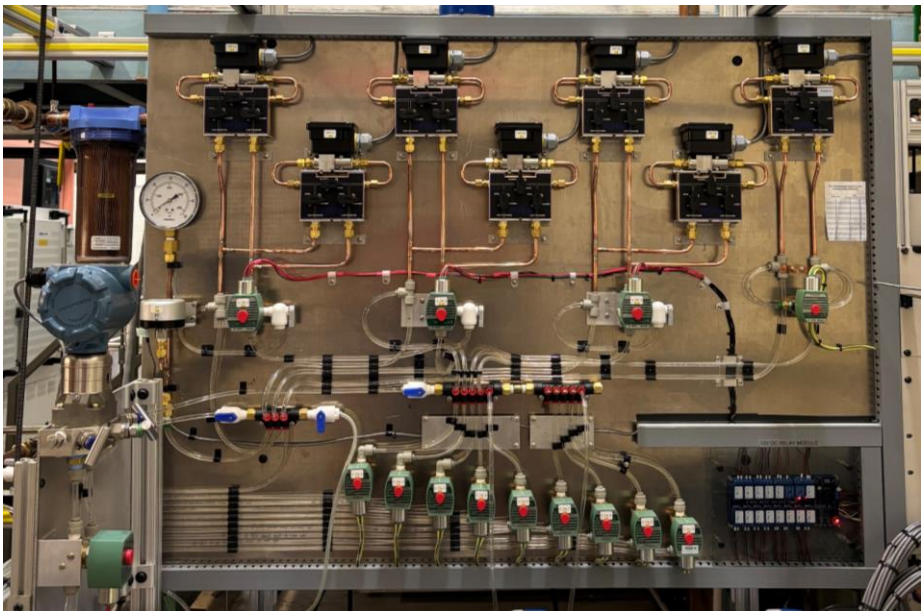

Figure 7. A photo of the pressure measurement panel.

4.1.1. Pressure Tap

Pressure taps are small holes on a pipe wall for measuring static pressure. The most important considerations of pressure taps are the size, depth, and edge condition. Detailed considerations have been discussed in [11–13].

The ideal tap should be perpendicular to the wall and have edges that are square with the wall surface, free from any burrs or irregularities. Having a hole with finite size will inevitably distort the flow to some degree and introduce a systematic error. While the error decreases with the hole size, excessively small holes are difficult to machine, vulnerable to blockage by fluid impurities, and relatively slow in pressure response. Practical hole sizes usually range between 0.5 mm and 3 mm [12]. The pressure error generally increases with the depth of the tapping cavity, but its impact is coupled with the size effect in a rather complex manner. Early measurements in [14, 15] showed that a depth-to-diameter ratio between 0.5 and 2.5 yields a relatively low error.

Counterbore and through holes are two typical configurations of static pressure tapping. Counterbore taps consist of a small hole facing the flow and a relatively large cavity behind it, which allows attachment for tubing with a larger diameter than the hole, thus leading to a faster pressure response than a through hole with the same tap size. However, counterbores are typically used in large pipes with relatively thick walls. The wall thickness of our test pipes ranges between 0.76 mm to 1.78 mm, which is not practical for boring counterbore holes. Hence, the pressure taps in this facility were bored through the pipe wall.

A diameter of 1.59 mm (1/16 in.) was chosen for all pressure taps. Since they are bored-through holes, their depths are fixed by the wall thickness (between 0.76 mm and 1.78 mm). This value gives a depth-to-diameter ratio between approximately 0.5 to 1, which is in accordance with the recommendation by [15].

Initially the holes were bored by a drill, which created burrs due to the drill cutting angle and speed. However, it was difficult to deburr in the middle of a long pipe using conventional methods like honing and polishing. One solution may be dividing the pipe into several shorter segments, but this would introduce new sources of error, such as pipe alignment and connection. Thus, an alternative technique that can bore burr-free holes was sought.

End milling was then used to make burr-free holes. An advanced milling technique–helical interpolation–was used, which involved simultaneous circular movement in the horizontal plane combined with a vertical feed at a distinct pitch. This approach was done in a computer numerical controlled (CNC) vertical milling center (Haas VF-3). An end mill bit of 0.81 mm (0.032-in.) diameter was used with a drop rate of 0.0002 per revolution. A ruby probe was used to assist the CNC in positioning and alignment of the taps in the X, Y, and Z axes within a tolerance of 0.0254 mm (0.001 in.). Figure 8 shows the holes in a test piece. The technique proved to be effective, with the resulting taps uniform and free from visible burrs. Thus, no honing or polishing was performed afterwards.

Figure 8. Pressure taps bored by end milling on a test piece.

The error due to minor imperfections of pressure taps are largely mitigated by two measures: 1) measuring pressures at various streamwise locations and using least-square regression to calculate the pressure gradient and the static pressure at the fitting location; 2) for each streamwise location, boring four taps uniformly spaced around the circumference to give an average static pressure. The four opposite facing taps are precisely aligned using a square collet block set with surface ground tolerance of 0.0127 mm (0.0005 in.).

4.1.2. Piezometer Ring

A piezometer ring connects the pressure taps in the same streamwise location and senses the average static pressure, serving to account for possible imperfections of pressure tap fabrication as well as pressure variations around the circumference. The latter effect is more significant in fittings that involve change of direction, such as elbows and tees.

Figure 9 shows three possible configurations of piezometer rings. The configurations (a) and (b) involve attaching a tube to a pressure tap directly, which is impractical in the pipe sizes and thicknesses of interest. The reason is three-fold: 1) if the tube is inserted to the tap, it is difficult to be flush with the inner wall surface, and even a slight degree of protrusion would introduce significant error; 2) if the tube is attached to the outer wall surface by soldering or brazing, the

solder would wick inside when heated, clogging the tube and tap; 3) regardless of how the tubing is attached, when soldering all the four tubes must be held in place at the same time, which is very difficult in practice. Therefore, configuration (c) is used, where the taps are connected to a common channel rather than individual tubing.

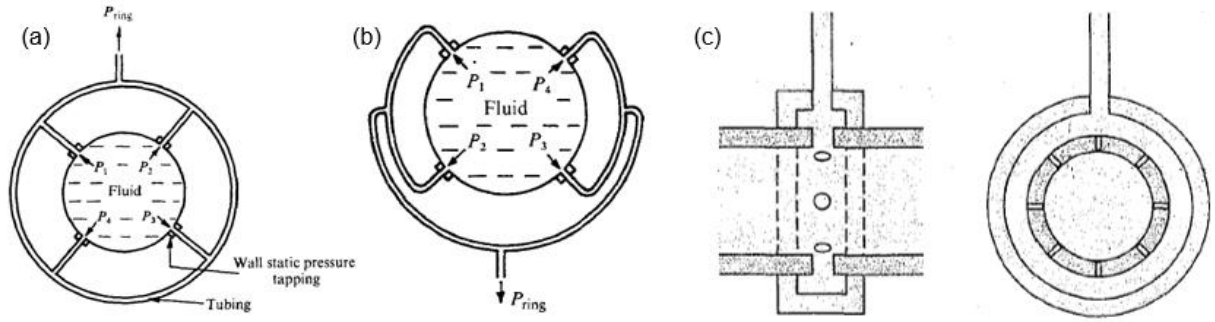

Figure 9. Possible configurations of piezometer ring: (a) conventional [16]; (b) "Triple-T" [16]; (c) present study.

The piezometer ring was initially machined from a single piece of brass block, as shown in Figure 10 (a). It is a brass sleeve that creates a common channel, and it has a 3.175 mm (1/8-in.) port to connect to the pressure transducer. It is challenging to attach the ring to the test pipe in that it needs to be soldered, during which the solder may wick into the common channel and the taps. To check this concern, we soldered the ring to a sample copper pipe and then cut it in half for inspection, as shown in Figure 10 (b) and (c). A considerable amount of solders was observed at the pressure taps, modifying the shape and edge condition. This design was therefore abandoned.

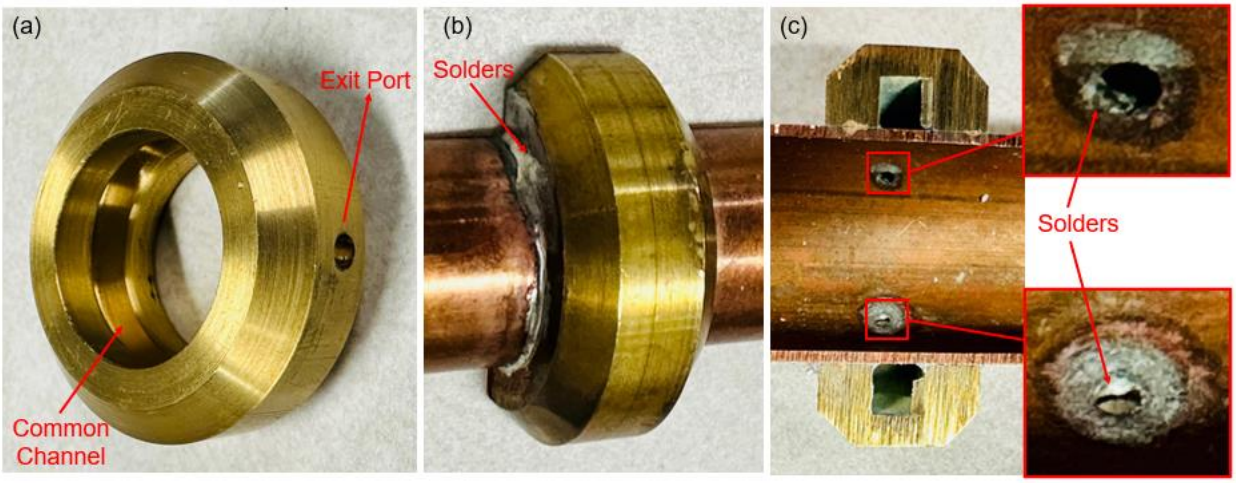

Figure 10. Initial design of piezometer ring (abandoned because the solder would wick into channels and pressure taps).

Figure 11 shows the second design of the piezometer ring. It was fabricated by simply milling a groove inside a commercial compression union fitting. The ring was mounted to the test pipe and sealed by compressing ferrules with nuts. A 6.15 mm (1/4-in.) hole was drilled halfway through the body of the compression union, where a short piece of copper tube was brazed, connecting the ring to a remote pressure transducer. The exit port was angled at 45° relative to the upper two pressure taps to minimize the potential pressure drop caused by the piezometer ring [17].

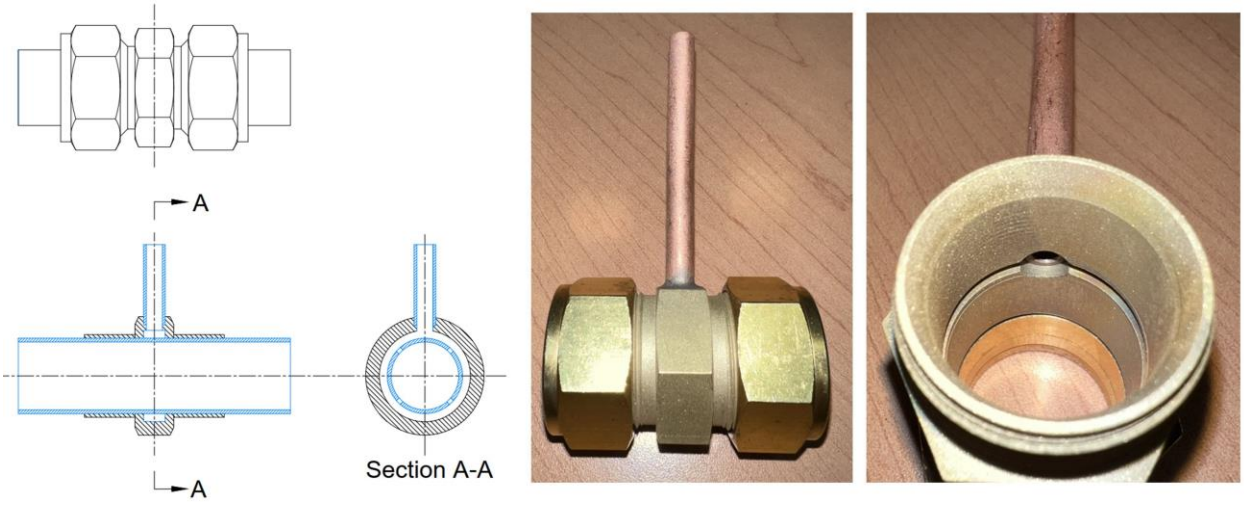

Figure 11. Second design of the piezometer ring.

4.1.3. Pressure Sensors

The static pressure at each piezometer ring is measured using differential pressure (DP) transducers or transmitters. All measured DPs are referenced to the most upstream piezometer, i.e., piezometer #1. A challenge to measure DP with consistent accuracy stems from the remarkably wide range of DP in our test conditions, which spans over four decades (log scale) from 6.9 Pa to 68.9 kPa (0.001 psi to 10 psi). This range can cause extremely large relative uncertainty in small DP measurement, because in general the accuracy of a DP sensor is consistent over its range and proportional to the full span (FS). For example, if a DP sensor with uncertainty of ± 0.25 %FS is used to measure the above DP range, the sensor's range will be (0 to 68.9) kPa (i.e., 0 to 10 psi), then the absolute uncertainty will be 68.9 kPa × 0.25 % = 0.17 kPa. When this sensor is used to measure a DP of 6.9 Pa, the absolute uncertainty remains the same, but the relative uncertainty will become 0.17 kPa / 6.9 Pa = 2500 %, which is unacceptable.

To address the challenge of measuring a wide range of DP, five sets of DP sensors of different range were used along with an automatic switching system that can select the most relevant range based on the DP to be measured (see Section 4.1.4 for details of the automatic switching system). Table 1 lists the key properties of the DP sensors. The smallest and largest DP ranges are 2.5 kPa (0.36 psi) and 68.9 kPa (10 psi), respectively. Note that DP0's lower range limit was

configured to be a negative value (-0.7 kPa). This selection is because the pump induces pressure fluctuation, and the instantaneous pressure can fall below zero when DP is very small. If the lower range limit is zero or above, the negative pressure signals will be cut off, resulting in inaccurate measurement of the mean pressure. In addition to DP0 and DP4, there are three sets of sensors with pressure range of (0 to 6.9) kPa (DP1), (0 to 13.8) kPa (DP2), (0 to 34.5) kPa (DP3), respectively, and each set consists of two identical sensors for instrument redundancy. The detailed manufacturer information of the DP sensors is given in Appendices A.4 and A.5.

The five sets of DP sensors divide the DP range into five bins: < 2.5 kPa, (2.5 to 6.9) kPa, (6.9 to 13.8) kPa, (13.8 to 34.5) kPa, and (34.5 to 68.9) kPa. This configuration avoids using a large-range, large-uncertainty sensor to measure a small DP, and hence avoid large relative uncertainty. The smallest possible DP, 6.9 Pa, is measured by the sensor DP0 that has the smallest range and uncertainty, resulting in a relative uncertainty of 11.5 % if only one sensor is used for all DP measurements. It is expected that DP = 6.9 Pa will be only encountered in extreme cases (i.e., smallest velocity and shortest distance); the DP in most test conditions will be greater than 1 kPa and hence the associated relatively uncertainty will be less than 0.1 %.

Table 1. Key specifications of the differential pressure transducers

Sensor Ref. ID	Unit	DP0	DP1a	DP1b	DP2a	DP2b	DP3a	DP3b	DP4
Pressure Range	kPa	-0.7 – 2.5	0 – 6.9	0 – 6.9	0 – 13.8	0 – 13.8	0 – 34.5	0 – 34.5	0 – 68.9
Pressure Range	Psi	-0.1 – 0.36	0 – 1	0 – 1	0 – 2	0 – 2	0 – 5	0 – 5	0 – 10
Accuracy [a]	%FS	0.025	0.25	0.25	0.25	0.25	0.25	0.25	0.25
Absolute Uncertainty [b]	Pa	0.8	17.2	17.2	34.5	6.9	21.4	13.1	32.4
Absolute Uncertainty	psi	0.000115	0.0025	0.0025	0.0050	0.0010	0.0031	0.0019	0.0047
Nominal Relative Uncertainty	%	0.06 [c]	0.37	0.37	0.33	0.07	0.09	0.05	0.06

[a] Stated by the manufacturer.
[b] Determined from calibration.
[c] For 0.001–0.36 psi.

The measurement function of a DP sensor is expressed as

$$P = a(V - V_0) \tag{5}$$

where P is the pressure reading; V is the transducer analog output (voltage or current); a is the slope, obtained from calibration (see Sec. 4.1.5); V_0 is the analog output at zero pressure, obtained from "auto-zero" process before each measurement (see Sec. 4.1.6). As the uncertainties of V and V_0 are negligibly small compared to that of a, the uncertainty of P can be calculated by:

$$u_P = u_a(V - V_0) \tag{6}$$

where u_a is obtained from calibration (Sec. 4.1.5).

4.1.4. Automatic Switching System

The automatic switching system has two functions: 1) scanning the pressure of each piezometer ring along the test section; 2) selecting the appropriate DP sensor based on the value of DP. The system is comprised of an arrangement of manifolds and solenoid valves, as shown in Figure 5. Each piezometer is controlled by a two-way solenoid valve that is normally closed. By switching on a solenoid valve, the pressure from piezometer #X (X = 2, 3, …, 9) is sampled and transmitted to DP sensors. A manifold (a.k.a. low-pressure manifold) is used to connect piezometers from #2 to #9 and the low sides of all DP sensors. Another manifold (a.k.a. high-pressure manifold) is used to connect piezometer #1 and the high sides of all DP sensors. Each DP sensor is controlled by a three-way solenoid valve, which connects the high side of the DP sensor, low side of the DP sensor, and the low-pressure manifold. When deenergized, the three-way solenoid valve opens the path between the high and low sides of the DP sensor, equalizing their pressures. This prevents a DP sensor from overpressure or trapping pressure. When energized, the three-way solenoid valve opens the path between the low side of the DP sensor and the low-pressure manifold, transmitting the pressure sampled from piezometer #X (X = 2, 3, …, 9) to the DP sensor, and allowing the sensor to sense the DP between piezometer #X and piezometer #1.

4.1.5. In-situ Calibration

The in-situ calibration system is used to verify the manufacturer's calibration of the DP transducers after installation or re-calibrate them if necessary.
The system consists of a pressure standard and a water column used as the pressure source. The pressure standard is a high-accuracy pressure transducer that is periodically sent to the manufacturer for calibration. It is a gauge-type pressure transducer, with full span of (0 to 68.9) kPa and uncertainty of 0.01 % FS or 6.9 Pa (95 % confidence interval), whichever is larger. Full specification of the pressure transducer is given in Appendix A.6. The column is made of a clear, hard polyvinyl-chloride (PVC) pipe with an inner diameter of 12.7 mm (1/2 in.) and length of approximately 3.7 m, with additional hoses attached to the bottom. The column is open to the atmosphere at the top, and its bottom is connected to the high-pressure sides of the pressure standard and the transducers to be calibrated, whose low-pressure sides are both open to the atmosphere. A three-way valve is used to switch the water column between draining and connecting to other transducers.

The calibration only determines the slope of the linear transfer function of pressure transducers, while the y-intercept is determined from "auto-zero" (Sec. 4.1.6). This approach simplifies the calibration system setup because the pressure standard needn't be installed at the exact same elevation as the transducer to be calibrated. An elevation offset doesn't affect the slope calibration. In this facility, the pressure standard is mounted at a location ~ 0.9 m lower than the transducers.

In the beginning of a calibration, the column is filled with water to a height that corresponds to a pressure not exceeding the largest upper limit of the pressure transducers to be calibrated. This action can be done by turning on the pump to push the water from the main loop into the column through the high manifold. If the transducers are previously filled with water, their low-

pressure ports should be drained and dried. The bleeding screw at the low-pressure side should be removed throughout the calibration to allow complete atmospheric exposure.

A calibration was done by intermittently draining the column to change the water height, thereby the pressure, generating a dataset of pressure (P_s) vs. analog output (V or I). The calibration for each DP transducer was repeated five times within a week. Figure 12 shows the calibration results for a representative transducer (DP3a). To check the repeatability, the data from different days were first separately linearly fitted. Overall, the data are very consistent. The slopes are within ± 0.8% of their mean, while the y-intercepts show a slight offset, which may be caused by temperature variation and repeatability errors. Since only the slope is of interest, the offsets were eliminated by subtracting the fitting y-intercept from each data set. The corrected data were combined and fitted to $V = \beta P_s$, where the y-intercept is fixed at zero. The resulting β was then used to determine the slope of the measurement function (Eq. 5): $a = \beta^{-1}$. The standard uncertainty of a was estimated by $u_a = \left[u_\beta^2/\beta^4 + u_{P_s}^2\right]^{0.5}$, where u_β is the standard uncertainty of β, obtained from the fit, and u_{P_s} is the standard uncertainty of the pressure standard.

One may wonder why not fit P vs. V directly, given that it readily gives the slope of the measurement function (Eq. 5), instead of fitting V vs. P and then inverting it. In fact, the latter seemingly more circuitous route is generally preferred in instrument calibration. This technique is preferred because least square regression assumes no error in x-axis variables and minimizes the error of the fit in the y-axis. Thus, the reference variable (pressure standard in this case), which is typically associated with much smaller error, should be on the x-axis to give a smaller overall error. A detailed discussion for a similar problem can be found in [17].

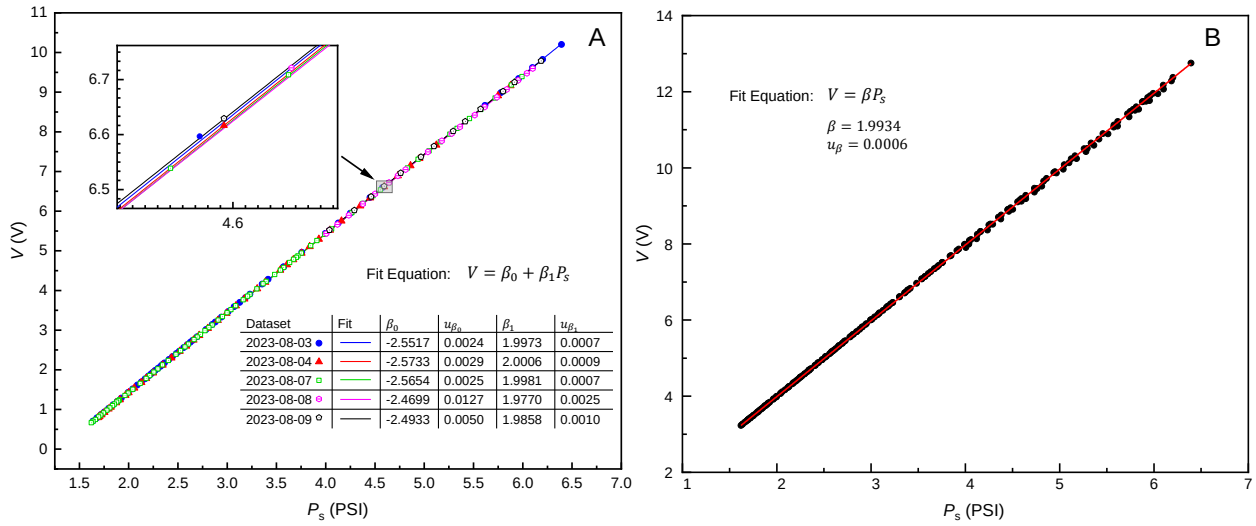

Figure 12. Calibration data for the pressure transducer DP3a. A) Individual datasets and curve fits; B) Combined dataset and curve fit.

4.1.6. Auto-Zero

An auto-zero process is a secondary calibration that provides an additional correction of output errors such as offset drifting. An auto-zero process is performed for all DP sensors before each set of experiments to determine the zero-pressure output (i.e., V_0 in Eq. 5). During the process, the pump is off, and all solenoid valves are deenergized. This step creates a known reference condition: DP = 0 for all DP sensors, because the high and low side of each DP sensor are automatically connected when the corresponding solenoid valve is deenergized, as explained in Sec. 4.1.4. The analog output of each DP sensor, V_0, is then measured for a sufficiently long period of time to ensure the uncertainties due to random error (u_{V_0}) are two magnitudes smaller than the uncertainty of the scaling factor (u_a). Here, $u_{V_0} = s_{V_0}/\sqrt{n_{V_0}}$, where s_{V_0} and n_{V_0} are the standard deviation and the number of the taken readings for V_0; u_a is obtained from the sensor calibration. The measured V_0 is then used to correct the DP measurements through Eq. 5.

4.1.7. Connection Tubing, Valves, and Fittings

Clear polyurethane tubing is used for impulse lines that transfer pressure. Polyurethane is chosen because it allows visible inspection of fluid, aiding the identification and removal of air pockets. In addition, polyurethane tubing is extremely flexible, resistant to kinking, and easy to cut. Push-to-connect fittings and valves are used extensively in the rig to connect the tubing. All these parts are inexpensive and very easy to install and to modify.

The tube OD and ID are 6.35 mm (1/4 in.) and 3.175 mm (1/8 in.), respectively. There is a tradeoff in selecting the tube ID. Smaller ID leads to shorter response times, but it also increases the likelihood of trapping air and blockage by impurities. In addition, the capillary effect will become significant when the diameter is below 2 mm (Figure 13), introducing error to the pressure measurement. The selection of 3.175 mm ensures that the capillary effect is insignificant. Note that this ID is smaller than the recommendation value of ISO 2186 [18], which is between 4 mm to 25 mm. However, ISO 2186 is intended for industrial applications where the fluids generally contain impurities and visual inspection is not possible. In our test facility, as the water is clean and is visualized through clear tubing, any trapped air or impurities can be identified and removed immediately. This capability allows us to use a smaller tubing to have a faster response in pressure measurement.

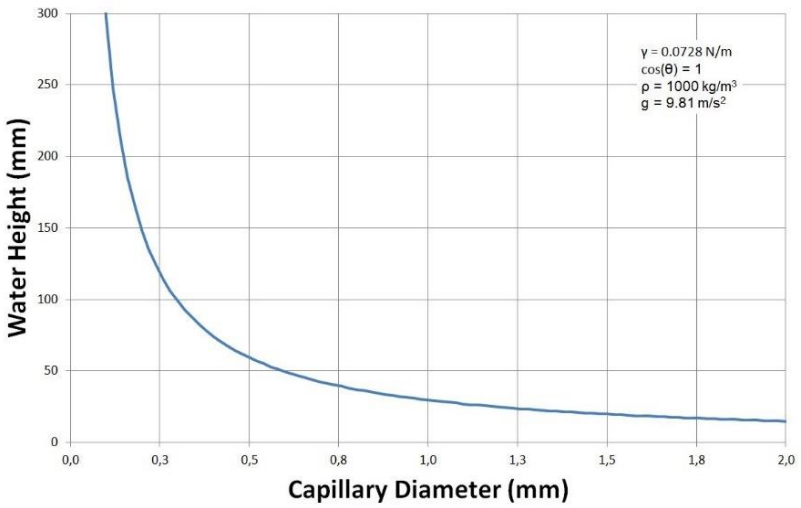

Figure 13. Effect of tube diameter on the capillary effect.

4.2. Flowrate and Density Measurements

Three Coriolis flowmeters with the same specification are used to measure the flowrate ($\dot{m}$) and the density (ρ) of the water. Their locations are shown in Figure 3. This arrangement ensures that there are always two independent measurements for the same flowrate or density, which reduces the measurement uncertainty when using their average as the result. The uncertainty of mass flowrate measurement of each Coriolis flowmeter, $u_{\dot{m}_0}$, is ± 0.05 % of the reading (for $\dot{m} \geq 0.264$ kg/s) or ± 0.95 kg/h (for $\dot{m} < 0.264$ kg/s). When two Coriolis flowmeters are used, the uncertainty can be calculated by $U_{\dot{m}} = \sqrt{2}U_{\dot{m}_0}/2$. While the Coriolis flowmeters are for the test section, a lower-cost ultrasonic flowmeter is used to measure total flowrate, in the test section and the bypass line. This measurement is primarily for monitoring and for feedback to the pump, and thus requires less accuracy. The uncertainty of the ultrasonic flowmeter is 0.5 % of reading plus 3.79 L/min (0.035 gallon per min). Detailed specifications of the flow meters are given in Appendices A.7 and A.8.

The uncertainty of density measurement of each Coriolis flowmeter, U_ρ, is ± 1 kg/m^3. By averaging the density measurement of two Coriolis flowmeters, the uncertainty is reduced to ± 0.707 kg/m^3. For checkup, density measurements are compared to calculation values based on measured temperatures (Sec. 4.3).

4.3. Temperature Measurements

Three PT100 resistance temperature detectors (RTDs) are used to measure the in-flow temperature near the inlet and outlet of the test section. Their locations are shown in Figure 3. The uncertainty of the RTD is: $U_{\mathrm{RTD}} = \pm\,(0.15\ +\ 0.002\ \times\ T)$ °C, which is in compliance with the IEC[1] Class A accuracy. The temperature result is taken as the average of the inlet and outlet

[1] International Electrotechnical Commission

RTD readings, and the associated uncertainty is $U_T = \sqrt{2}U_{\mathrm{RTD}}/2$. Each RTD probe is 3.175 mm (1/8 in.) thick and is attached to the pipeline using a tee along with a bore-through Swagelok adapter. The probe's tip is inserted to the center of the pipe to ensure best contact of the fluid. Detailed specifications of the RTD are given in Appendix A.9.

The measured temperature is used to calculate the viscosity and the density of water. The calculation was done using REFPROP 10 [19]. The uncertainty of the calculated density is 0.0001%, and the uncertainty of the calculated viscosity is 3%.

4.4. Data Acquisition and Measurement Automation

A data acquisition (DAQ) system is used to acquire data from the above sensors and control the equipment (i.e., the centrifugal pump, solenoid valves, etc.). The DAQ system has several input modules for measurements of current, voltage, frequency (or pulses), and resistance. In addition, the DAQ system has a digital output module and an analog output module for control.

All modules are plugged in to a compact, 8-slot chassis that integrates signal connectors, signal conditioning, and analog-to-digital converters (ADC). The chassis is connected to a lab computer through Ethernet. Detailed specifications of the DAQ system are given in Appendix A.10.

An in-house LabVIEW program has been developed to (i) drive the DAQ system, (ii) configure and automate the measurement process, and (iii) display and record data. A graphical user interface (GUI) was developed to enable interactive experiment configuration and data analysis. Figure 14 shows two snapshots of the GUI.

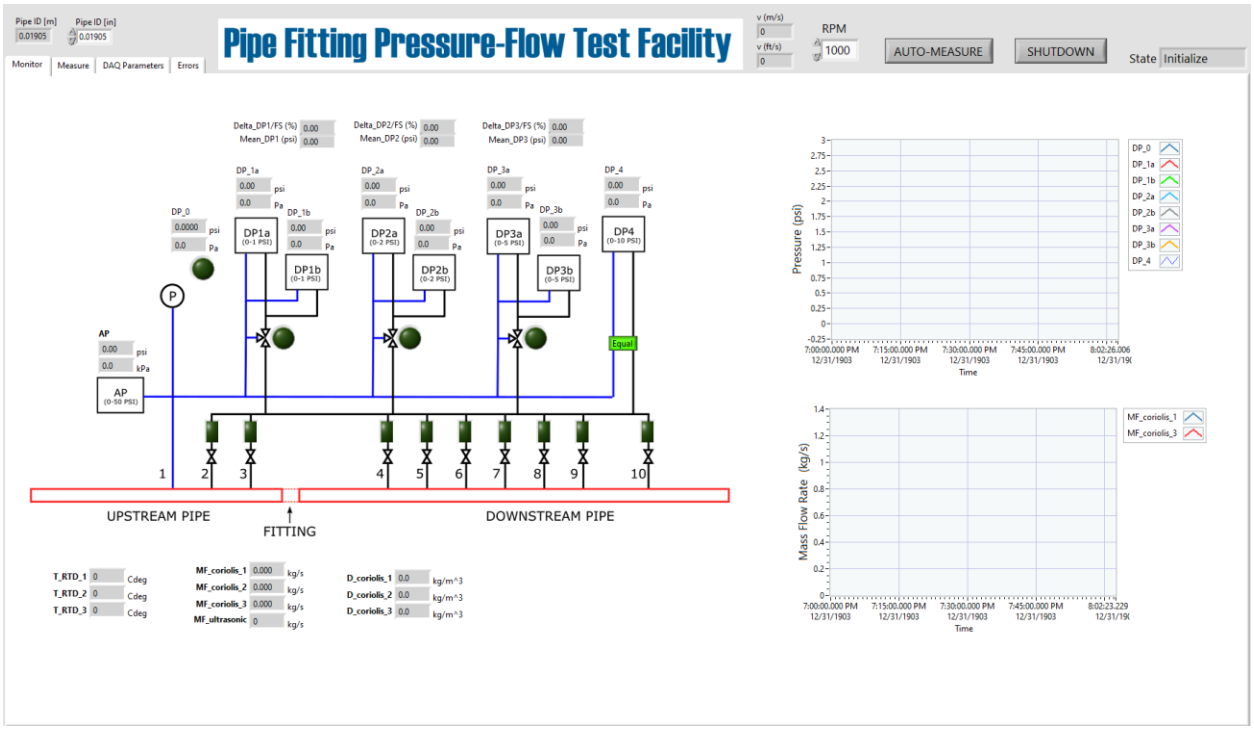

(a) Monitor mode

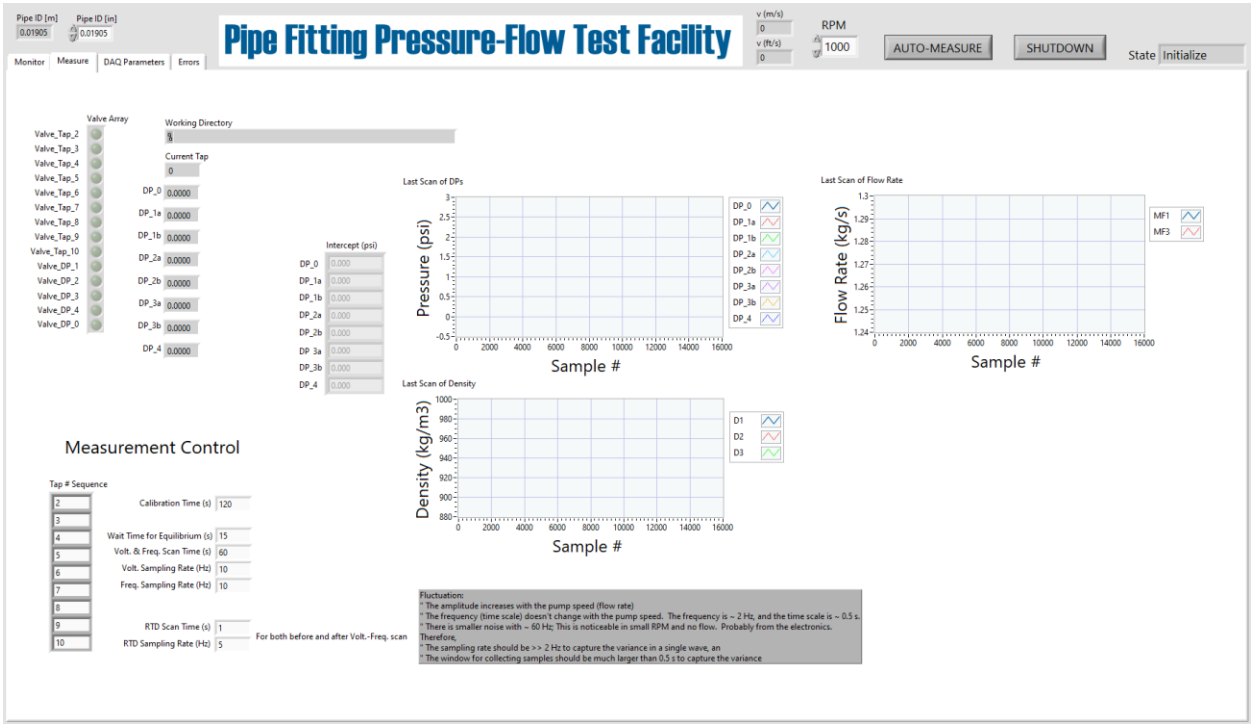

(b) Measurement mode

Figure 14. Snapshots of the GUI of the LabVIEW program.

The general workflow of each experiment has the following four stages:

1) Initialization. The program configures the experimental parameters based on user inputs or default values and then initializes the DAQ system and schedules the measurements.

2) Auto-Zero (described in Section 4.1.6).

3) Monitor. As shown in Figure 14 (a), the real-time measurements of pressure and flowrate are displayed in graphs and values. All solenoid values can be manually controlled by clicking the corresponding buttons in the GUI. Typically, after starting the pump or changing the pump speed, the flowrate is closely monitored until it reaches steady state, and then the system is ready to enter the measurement mode.

4) Measurement. In this mode, the DPs for all piezometers are scanned one by one, following the preset scanning sequence. The scanning sequence, as well as other measurement control parameters (e.g., the length of each DP measurement process, the length of RTD measurement process, the equilibrium waiting time, and the sampling rates of different sensors), is input in the GUI under the tab “Measure” (see Figure 14 (b)) and can be changed when it is not scanning. As shown in Figure 15, while scanning for a piezometer, DP4 is first used to provide a “rough” measurement, then a determination is performed of which other DP with appropriate and smaller range will be selected to perform a “fine” measurement. The default scanning time and sampling rate are 60 s and 10 Hz, respectively. The switching between DP sensors is done by the solenoid valves, as discussed in Section 4.1.4. A waiting period (15 s by default) is set in place after the switch to allow the pressure and flow to reach equilibrium. The flowrate is measured concurrently with the pressure measurement. This simultaneous measurement is possible because the signals of flowrate and pressure are frequency and analog (current/voltage), respectively, which use different ADC in the DAQ. However, RTD measurements use the same ADC as that of pressure, and hence are done before and after the pressure measurement, and the average is used as the temperature corresponding to the pressure measurement (see Sec. 5.3 for more discussion).

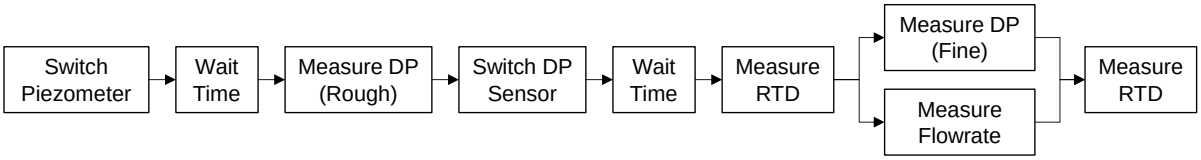

Figure 15. Schematic of a single scan for a piezometer.

5. Validation Tests for a Straight Pipe

A set of tests were performed for a straight pipe to verify the instrumentation and measurement methods. The test pipe is a NTS ¾, Type L copper pipe. The inside diameter was measured to be 20.11 mm (0.791 in.). It was cut into a 5-ft and a 7-ft pieces, connected by a SharkBite coupling. Table 2 shows the streamwise locations of the pressure taps in the test pipe. To eliminate the impact of the coupling and to have adequate length for flow development, only downstream pressure taps were used for analysis. For each tap,

Table 2. Location (*z*) of pressure taps in the current test pipe (NTS ¾) *

Number	Type	Location [m]	Number of Diameters
1	Upstream	-0.4572	-24
2	Upstream	-0.2667	-14
3	Upstream	-0.0762	-4
4	Downstream	0.3810	20
5	Downstream	0.5715	30
6	Downstream	0.7620	40
7	Downstream	0.9525	50
8	Downstream	1.1430	60
9	Downstream	1.3335	70
10	Downstream	1.7145	90

* Locations are relative to the fitting (i.e., at the fitting, *z* = 0)

5.1. Pressure fluctuation

The use of a pump introduces pressure fluctuation. Figure 16 shows two series of DP signal for different pump speeds. It shows that the fluctuation amplitude increases with the pump speed (or flow rate). However, the fluctuation frequency doesn't change with the pump speed. The frequency is ~ 2 Hz, and the time scale is ~ 0.5 s. There is also a smaller noise of ~ 60 Hz, which is noticeable in small pump speed (Figure 16) and no flow. The 60 Hz noise may come from the electronics. Therefore, the sampling rate should be larger than 2 Hz to capture the variance in a single wave, and the sampling time for a single pressure measurement should be much larger than 0.5 s to capture the variance between the waves. The standard uncertainty of the pressure measurement can be evaluated by the standard deviation of the mean: $\sigma/\sqrt{N}$, where σ is the standard deviation, N is the number of samples. As N increases, the standard uncertainty decreases. Thus, by taking sufficient samples, the standard uncertainty can be negligibly small, and a rather accurate measurement of the mean value can be obtained, despite the fluctation.

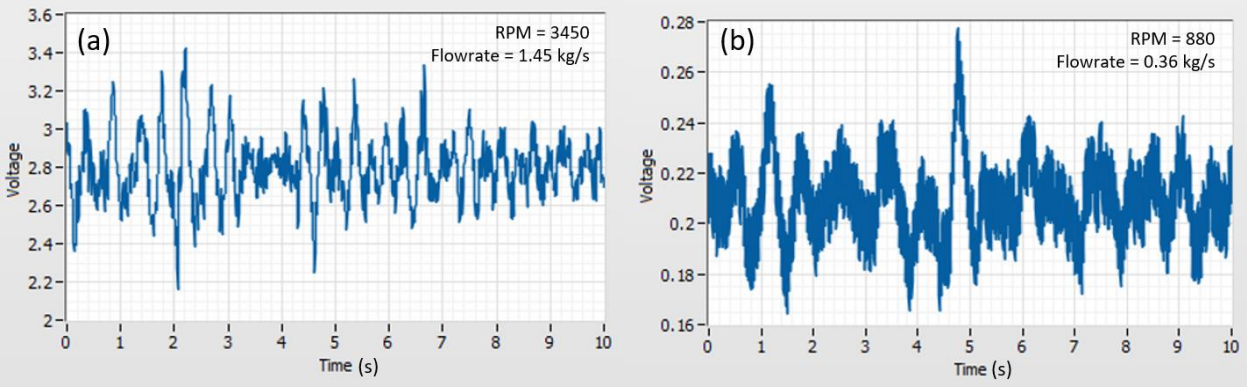

Figure 16. Pressure signals (in voltage) for different pump speeds (in RPM). The pressure tap location is #10. The sampling rate is 500 Hz.

5.2. Pressure distribution measurement

The pressure distribution was obtained from a sequential measurement of static pressure for different streamwise locations. For each pressure measurement, the sampling rate was 10 Hz, and the sampling time was 60 s, resulting in 600 samples. Figure 17 shows a typical measurement result. The insert of Figure 17 shows the pressure data of all samples for a particular location. Despite the fluctuation, the standard uncertainty (i.e., standard deviation of the mean) is very small—0.012 kPa, which is 0.4 % of the mean value. The uncertainty for other conditions are similar, all within 0.5 %. When the uncertainty was plotted in Figure 17 in error bars, the size was smaller than that of the symbols and are invisible. The static pressures along the pipe were linearly fitted to find the hydraulic grade line, as shown in the solid line in Figure 17. The 95 % confidence interval is also plotted in Figure 17, but it nearly coincides with the fitting line and is difficult to see. The standard deviation of the fit is 0.0046 kPa—0.14% of the mean.

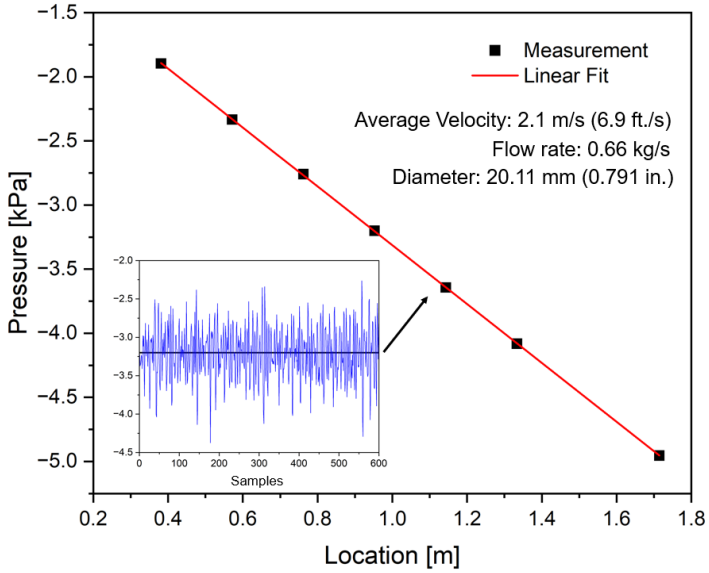

Figure 17. Typical result of pressure distribution measurement (Insert: pressure measurement for a single location, with sampling rate of 10 Hz and sample time of 60 s)

5.3. Friction factor

The friction factor can be calculated from the slope of a hydraulic grade line. Figure 18 shows the friction factor of all test conditions, including four repeated tests. The measured friction factors were compared to the Colebrook correlation [20], which is a well-established equation that yields friction factor as a function of Reynolds number, pipe diameter, and surface roughness. The surface roughness is estimated as 0.0015 mm, based on the recommended value for copper [21]. The measurements show excellent repeatability and agree well with the Colebrook correlation (within ± 3 %).

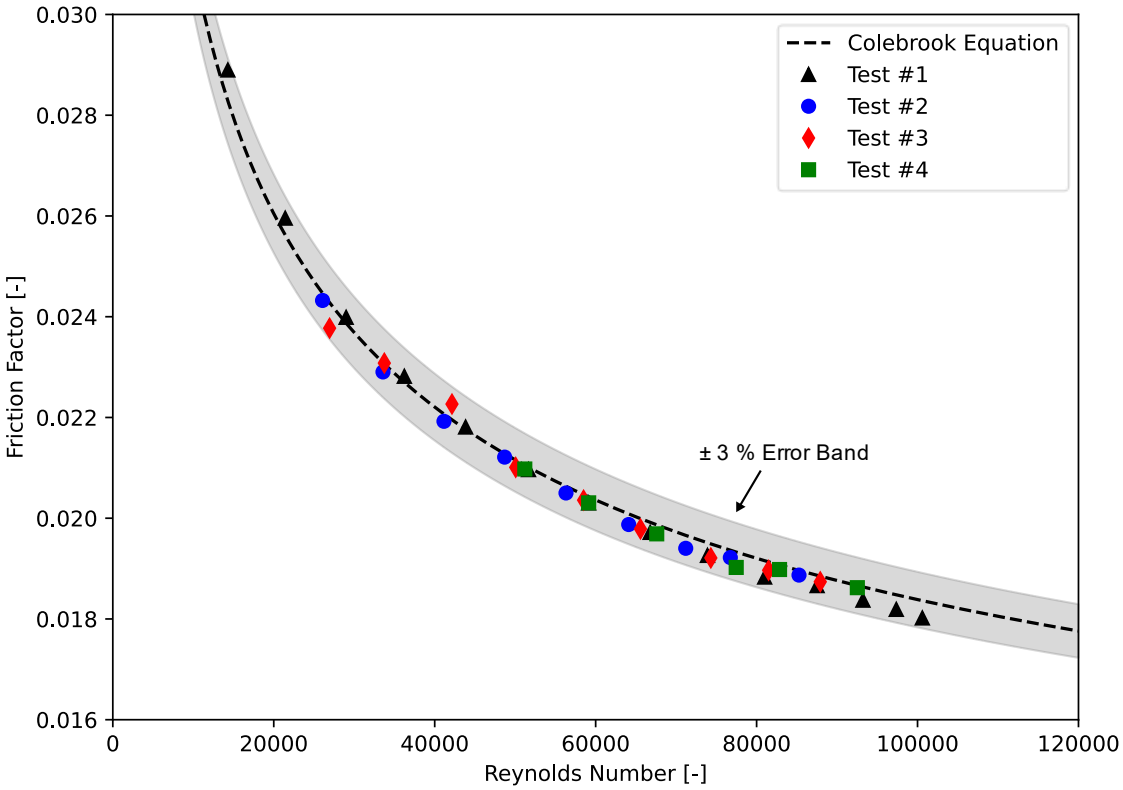

Figure 18. Measured friction factor in a straight copper pipe (ID = 20.11 mm).

5.4. Flow and Temperature Variation

As the pressure distribution is measured sequentially, it is important to maintain the same flow condition during the measurement. The flow condition is characterized by the Reynolds number (Re):

$$\mathrm{Re} = \frac{\rho V D}{\mu} \tag{7}$$

wherein,

ρ - Density
V - Average velocity
D - Pipe diameter
μ - Viscosity

The density and viscosity are functions of the temperature. Thus, for a certain pipe diameter and fluid, Re is influenced by the velocity and the temperature. As shown in Figure 19 (a), the velocities are very consistent during the pressure distribution measurements—the standard deviations are within 0.05%. Then, the flow condition mainly depends on the temperature variation.

There is no active temperature control in the test facility at this stage. As the pump and fluid friction generate heat, the water temperature can vary with the location, the time, and the flow condition to different degrees. Here, the water temperature is measured by two RTDs placed at the inlet and the outlet of the test section, respectively. The difference between the inlet and outlet temperatures is within 0.05 °C for all test conditions. Thus, the spatial variation along the test pipe can be neglected, and the average of the inlet and outlet temperatures is used to evaluate the water temperature.

Figure 19 (b) shows the temperature variation during pressure distribution measurements. In Figure 19 (b), each line represents an individual pressure distribution measurement for a certain flow condition; each point represents a single scan for a streamwise location, where the error bar represents the variation in a single scan—the two bar ends are the temperatures measured before or after the scan, respectively. As shown in Figure 19 (b), most errors bars are smaller than the symbol size, indicating the temperature variation in a single scan is very small. For all test conditions, the temperature variation in a single scan is within ± 0.15 °C. On the other hand, the temperature variation during a pressure distribution measurement is also small (i.e., within 0.3 °C) when $V \leq 3.6$ m/s (or 12 ft/s); when $V = 4.5$ m/s (15 ft/s), the temperature increased by 0.9 °C during the measurement, which is due to the increased pumping power.

Figure 19 (c) shows the variation of Re during pressure distribution measurements. For $V \leq 3.6$ m/s (or 12 ft/s), the Re variation in a single pressure distribution measurement is within 0.7 %; when $V = 4.5$ m/s (15 ft/s), the Re variation is within 2 %.

The temperature variation across different flow conditions is less of a concern. The temperature effect is incorporated into Re, and the pressure loss characteristic parameters (e.g., friction factor, pressure loss coefficient) scale with Re. Thus, when changing to a new flow condition (e.g., by changing the pump speed), the objective is typically to achieve a different Re, which doesn't require the same temperature as the previous one. Figure 20 shows the temperatures for tests of different velocities. The significant temperature variation is mainly due to heat generated by different pump speeds. Such variation doesn't affect the accuracy of the friction factor (refer to Figure 18)

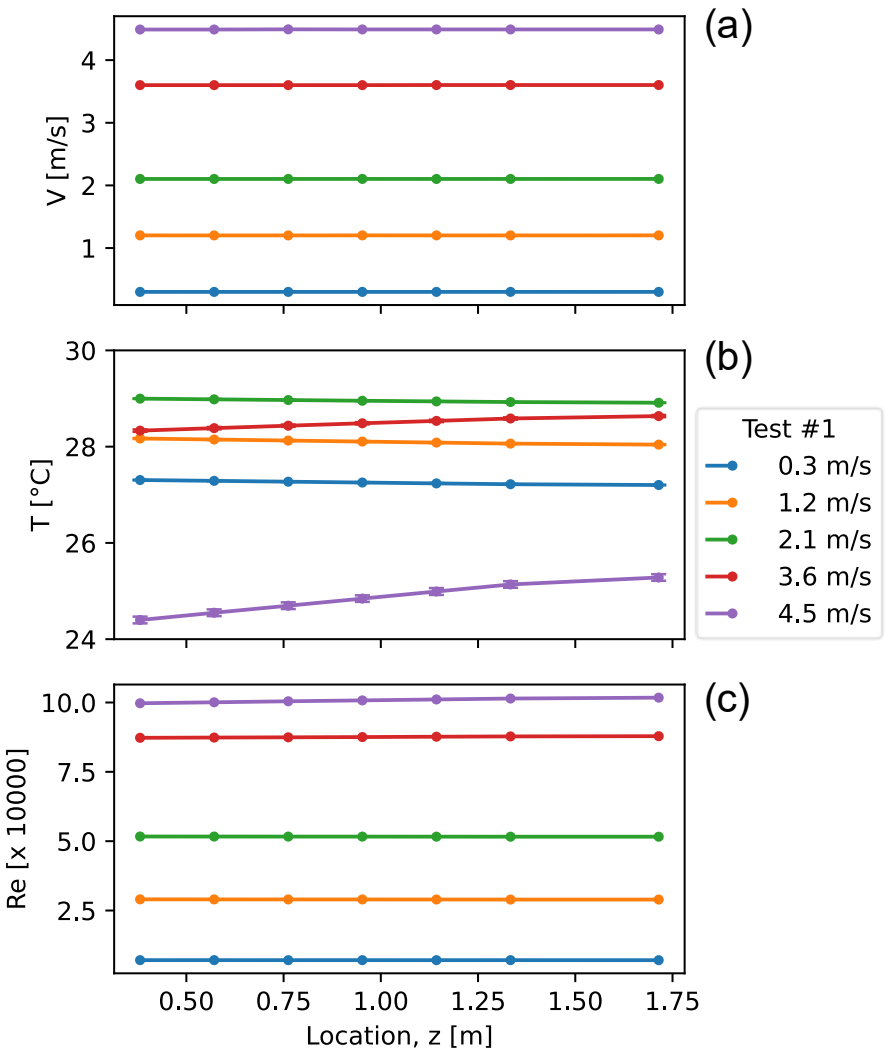

Figure 19. Variations of average velocity (V), temperature (T), and Reynolds number (Re) during a set of pressure distribution measurement.

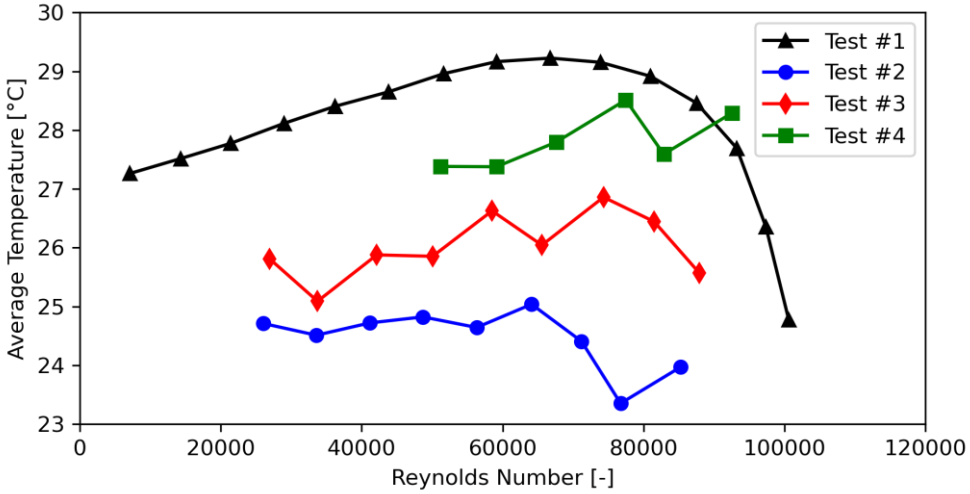

Figure 20. Variation of temperature among different flow conditions.

6. Summary

The NIST Plumbing Hydraulics Laboratory has been designed and built to test plumbing fittings in residential and small commercial applications. The measurement principle is that pressure losses in pipes and fittings can be accurately determined by establishing the pressure distribution, or the “hydraulic grade line”, which can be obtained by measuring the static pressure at several different locations along the pipe. The test facility is designed to measure the pressure loss for a variety of fitting types (couplings, elbows, tees and crosses), materials (copper, PEX, CPVC), and diameters (up to 2.54 cm or 1 in.) over a range of flow velocity from 0.30 m/s and 4.57 m/s (1 ft/s to 15 ft/s). The measurement is fully automated, enabled by an arrangement of sensors and solenoid valves controlled by a DAQ system and LabVIEW. Lessons learned from the design process are presented in this report including pressure tap design, piezometer ring design, in-situ calibration, and preprocessing data.

Several tests have been carried out for a straight pipe (NTS ¾, Type L, copper) to validate the method and the instrumentation. The measured friction factors show excellent repeatability and are within ± 3 % of the Colebrook correlation. The use of a pump introduces pressure fluctuation, which can be mitigated by averaging over sufficient samples. Additionally, the pump tends to increase the water temperature during the measurement. The temperature effect on the measurement of pressure loss parameters is generally insignificant, except for very high flow rate conditions.

References

[1] Whipple GC, Carson HY, Hansen AE, Groeninger WC, Murphy WC, Gries JM, Thompson GN, Hunter RB Recommended minimum requirements for plumbing: report of subcommittee on plumbing of the building code committee. (Washington, DC).
[2] National Institute of Building Sciences (2022) 2022 Moving Forward: Findings and Recommendations from the Consultative Council.
[3] National Institute of Building Sciences (2016) 2016 Moving Forward: Findings and Recommendations from the Consultative Council.
[4] Lin L, Batista MD, Ferretti NM (2022) State-of-the-art review on measurement of pressure losses of fluid flow through pipe fittings. https://doi.org/10.6028/NIST.TN.2206
[5] Persily AK, Batista MD, Healy WM, Kedzierski MA, Lin L, Milesi-Ferretti NS, Ullah T, Yashar DA, Zimmerman S (2023) November 2022 NIST Premise Plumbing Research Workshop: Summary and Findings. https://doi.org/10.6028/NIST.TN.2256
[6] Giesecke FE, Badgett WH (1932) Loss of head in copper pipe and fittings. (939):529–542.
[7] Rahmeyer WJ (1999) Pressure loss coefficients of threaded and forged weld pipe fittings for ells, reducing ells, and pipe reducers. *ASHRAE Transactions* 105:334–354.
[8] Rahmeyer WJ (2002) Pressure loss data for large pipe ells, reducers, and expansions. *ASHRAE Transactions* 108:360–369.
[9] Rahmeyer WJ (2003) Pressure Loss Data for PVC Pipe Elbows, Reducers, and Expansions. *ASHRAE Transactions*:230–251.
[10] VORTAB Company (2019) *VORTAB Flow Conditioners*.
[11] McKeon BJ, Engler RH (2007) Chapter 4. Pressure Measurement System. *Springer Handbook of Experimental Fluid Mechanics* (Springer-Verlag, Berlin), pp 197–214.
[12] Tavoularis S (2005) *Measurement in Fluid Mechanics* (Cambridge University Press, New York, NY, USA).
[13] ASME PTC 19.2 (2010) Pressure Measurement.
[14] Shaw R (1960) The influence of hole dimensions on static pressure measurements. *Journal of Fluid Mechanics* 7(4):550–564. https://doi.org/10.1017/S0022112060000281
[15] Livesey JL, Jackson JD, Southern CJ (1962) The Static Hole Error Problem. *Aircraft Engineering and Aerospace Technology* 34(2):43–47. https://doi.org/10.1108/eb033517
[16] Blake KA (1976) The design of piezometer rings. *Journal of Fluid Mechanics* 78(2):415–428. https://doi.org/10.1017/S0022112076002504
[17] Ghosh A, Sparrow E, Gorman J (2018) Fluid-mechanic interactions between a pipe flow having circumferential pressure variations and a piezometer ring. *International Journal of Numerical Methods for Heat & Fluid Flow* 28(10):2284–2306. https://doi.org/10.1108/HFF-07-2017-0277
[18] ISO 2186 (2007) Fluid flow in closed conduits — Connections for pressure signal transmissions between primary and secondary elements.
[19] Lemmon EW, and Ian H. Bell, Huber ML, McLinden MO (2018) *NIST Standard Reference Database 23: Reference Fluid Thermodynamic and Transport Properties-REFPROP, Version 10.0, National Institute of Standards and Technology*. https://doi.org/10.18434/T4/1502528
[20] Colebrook CF (1939) Turbulent Flow in pipes, with particular reference to the transition

region between the smooth and rough pipe laws. *Journal of the Institution of Civil Engineers* 11(4):133–156. https://doi.org/10.1680/ijoti.1939.13150

[21] Çengel YA, Cimbala JM (2006) *Fluid Mechanics - Fundamentals and Applications* (McGraw-Hill).

Appendix A. Equipment Specifications

Disclaimer: Certain commercial equipment, instruments, or materials are identified in this paper in order to provide adequate experimental details. Such identification is not intended to imply recommendation or endorsement by the National Institute of Standards and Technology, nor is it intended to imply that the materials or equipment identified are necessarily the best available for the purpose.

A.1. Flow Conditioning Elbow

Manufacturer	VORTAB Company
Model Series	VEL
P/N	VEL-01.00-2-5-0-2
Pipe Size	2.54 cm (1 in.) Standard Schedule 40
Material	316 SS
Process Connection	ANSI 150 Flange
Dimensions	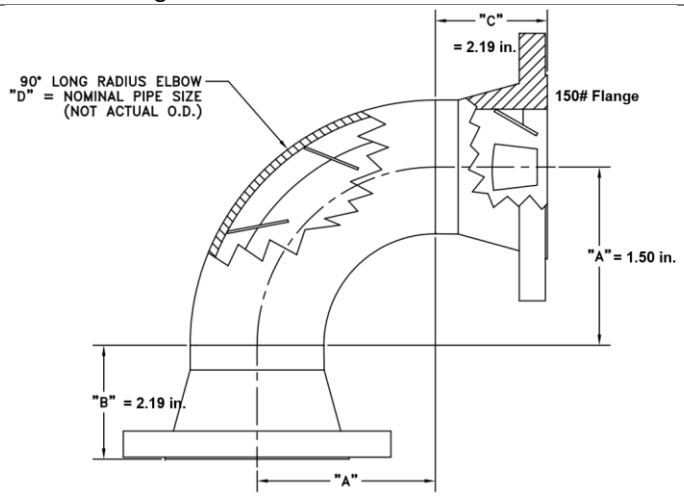

A.2. Centrifugal Pump

Manufacturer	Goulds Water Technology
Model Series	NPE
Product Code	1ST1H9A4
Motor	3-Phase, 2-Pole, Totally Enclosed, Fan-Cooled (TEFC)
Frequency	60 Hz
Supply Voltage	208-230 V
Power	3.0 HP
Suction Line Size	3.18 cm (1-1/4 in.)
Discharge Line Size	2.54 cm (1 in.)
Impeller Diameter	15.56 cm (6-1/8 in.)
Max. RPM	3500
Max. Head	47 m (at 3500 RPM)
Max. Pressure	9 bar (125 psig.)
Max. Temperature	121 °C

Hydraulic Performance Data	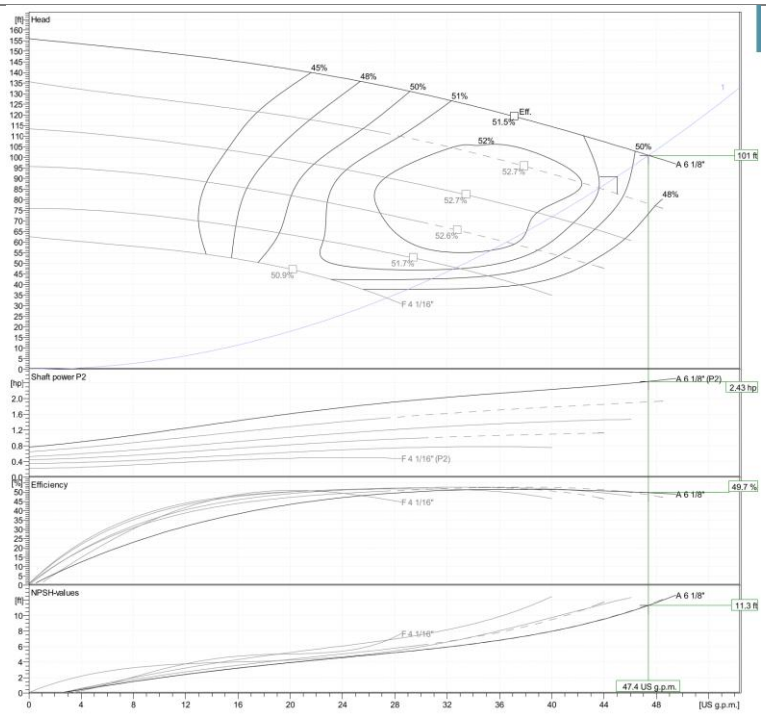

A.3. Variable Frequency Drive

Manufacturer	ITT Goulds
Model Series	Pumpsmart PS220
Product Code	K03550A04
Motor	3-Phase, Totally Enclosed, Fan-Cooled (TEFC)
Max. Motor Cable	300 m (984 ft)
Power	3.0 HP
Supply Voltage	208-240 V
Max. Current	10.1 A Continuous
Fuse Size	600V, 20A, Bussmann# JJS-20, Type T
Drive Platform	ABB ACS880-01
Drive Frame Size	R1
Weight	6.8 kg (15.0 lb)
Enclosure Rating	NEMA 1 / IP21

Dimensions	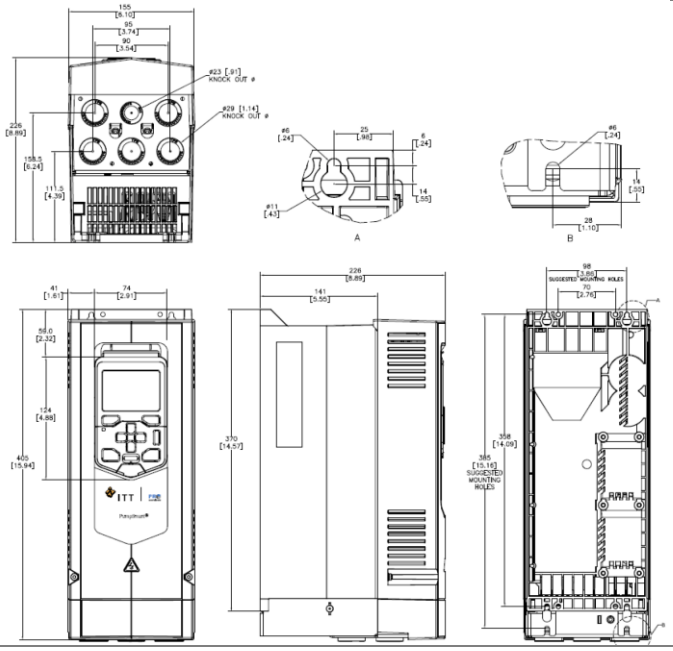

A.4. Differential Pressure Transducer (DP0)

Manufacturer	Emerson Rosemount
Model Series	3051S
Product Code	3051S1CD1A2A11A1AQ4 (Sensor + Transmitter)
Pressure Range	(-6.2 to 6.2) kPa, or (-25 to 25) inH_2O, allowing up to 200:1 rangedown
Accuracy	± 0.025 % FS
Isolating Diaphragm Material	316L SS
Electrical Output	(4 to 20) mA
Response Time	255 ms from the sensor module (physical limit, unconfigurable) plus 400 ms from the analog module (configurable from 0 – 60 s)
Long-term Stability	± 0.15 % of URL for 15 years
Ambient Temperature Effect	± (0.1 % of URL + 0.25 % span) from 1:1 to 50:1, per 28 °C
Line Pressure Effect	± 0.25 % of URL per 68.95 bar (1000 psi)
Mounting Position Effect	Zero shifts up to ± 0.00311 mbar, which can be zeroed span, i.e., no effect
Vibration Effect	< ± 0.1 % of URL when tested per the requirements of IEC60770-1 field or pipeline with high vibration level (10 Hz to 60 Hz 0.21 mm displacement peak amplitude/60–2000 Hz 3g)
Power Supply Effect	< ± 0.005 % of calibrated span per volt change in voltage at the transmitter terminals
Manifold	Model 305 Integral Manifold (R305EC32B11)

A.5. Differential Pressure Transducer (DP1 – DP4)

Manufacturer	Setra
Model Series	230, True Wet-to-Wet Differential Pressure Transducer
Product Code	2301001PD3V2EB, 2301002PD3V2EB, 2301005PD3V2EB, 2301010PD3V2EB
Type	Capacitive

Pressure Range	DP1: (0 to 6.9) kPa, or (0 to 1) psi DP2: (0 to 13.8) kPa, or (0 to 2) psi DP3: (0 to 34.5) kPa, or (0 to 5) psi DP4: (0 to 68.9) kPa, (0 to 10) psi		
Proof Pressure		High Side	Low Side
	DP1:	345 kPa (50 psi)	17 kPa (2.5 psi)
	DP2:	345 kPa (50 psi)	34 kPa (5 psi)
	DP3:	689 kPa (100 psi)	86 kPa (12.5 psi)
	DP4:	689 kPa (100 psi)	172 kPa (25 psi)
Accuracy, combining non-linearity, hysteresis, and non-repeatability	± 0.25 % FS		
Compensated Temperature Range	(-1 to 65) °C		
Zero Shift %FS per 50 °C	1.8		
Span Shift %FS per 50 °C	1.8		
Line Pressure Effect	Zero shift ± 0.004 % FS/PSIG line pressure		
Resolution	Infinite, limited only by output noise level (0.02 % FS)		
Static Acceleration Effect	2 % FS/g (most sensitive axis)		
Natural Frequency	500 Hz (gaseous media)		
Warm-up Shift	± 0.1 % FS total		
Response Time	(30 to 50) ms		
Long Term Stability	0.5 % FS per year		
Max. Line Pressure	2.4 MPa (350 psi), gauge		
Operating Temperature of Electronics	(-18 to 80) °C		
Electrical Output	(0 to 10) VDC		
Output Impedance	100 Ω		
Excitation	(13 to 30) VDC		
Electrical Circuit	3-Wire		
Dimensions (Sensor Only)	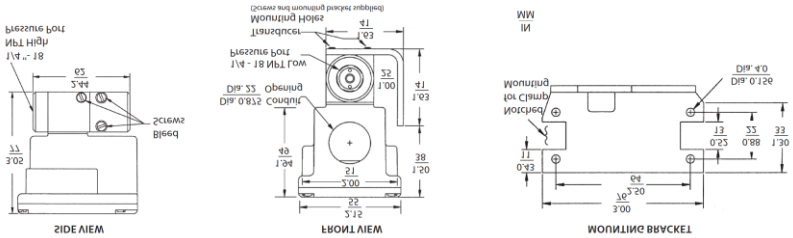		

Dimensions (With Manifold)	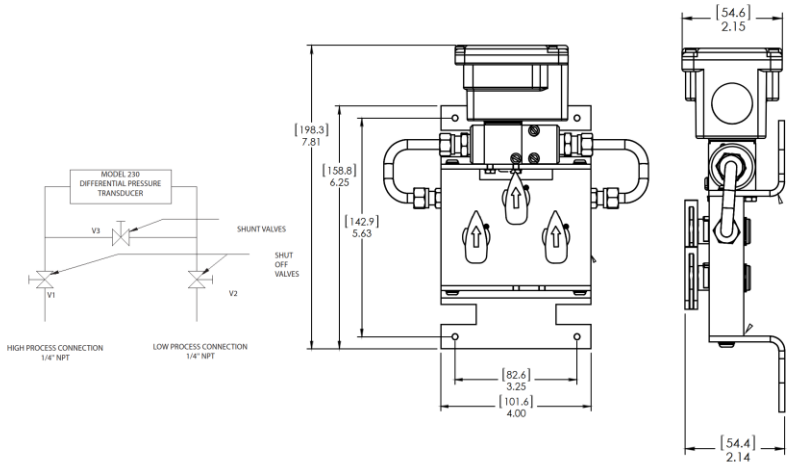

A.6. Gauge Pressure Transducer

Manufacturer	MENSOR
Model Series	CPT6100
Pressure Range	(0 to 68.9) kPa, or (0 to 10) psi
Accuracy	± 0.01 % FS
Communication	RS-232
Baud Rate	9600
Output Rate	50 Hz (20 ms)
Calibration Stability	Better than ± 0.01 % FS for 180 days with periodic re-zeroing
Overpressure Limit	150 % FS
Compensated Temperature Range	(15 to 45) °C
Operating Temperature Range	(0 to 50) °C
Storage Temperature Range	(-20 to 70) °C
Warm-up Time	15 min
Power	12 VDC ± 10 %, 55 mA max

A.7. Coriolis Flowmeter

Manufacturer	KROHNE
Model Series	OPTIMASS 6000F 25F (Standard, Remote Version)
Serial Number	U210000007400062, U210000007400063, U210000007400064
Transmitter	MFC 400
Measured Values	Mass, density, temperature
Calculated Values	Volume, referred density, concentration, velocity
Material	316L SS
Temperature Range	(-50 to 400) °C
Max. Pressure	100 bar (gauge) at 20 °C
Nominal Flow Rate	19000 kg/h
Max. Flow Rate	150 % of nominal flow rate
Nominal Accuracy	≥ 5 % of nominal flow: ± 0.1 % of actual measured flow rate < 5 % of nominal flow: ± zero stability (< 0.95 kg/h) 5 % of nominal flow = 950 kg/h = 0.264 kg/s
Zero Stability	< 0.95 kg/h for standard temperature

	< 1.52 kg/h for high temperature
Temperature Effect on Mass Flow Rate	0.00075 % of nominal flow per 1°C
Pressure Effect on Mass Flow Rate	-0.005 % of reading per 1 bar (gauge)
Calibration Accuracy	0.035 % overall -0.042 % at 1844 kg/h -0.012 % at 8582 kg/h -0.003 % at 15265 kg/h
Density Measuring Range	(100 to 3000) kg/m^3
Base Density Accuracy	± 1 kg/m^3
Density Repeatability	± 0.3 kg/m^3
Temperature Effect on Density	< 0.015 g/L per 1°C
Pressure Effect on Mass Flow Rate	+ 0.017 kg/m^3 per bar
Temperature Error	± 0.5 °C ± 0.5 % of reading
Weight (Sensor)	20.7 kg
Dimensions	A = 29.2 cm (11.5 in.) B = 63.2 cm (24.9 in.) E2 = 23.9 cm (9.4 in.) F = 11.7 cm (4.6 in.) 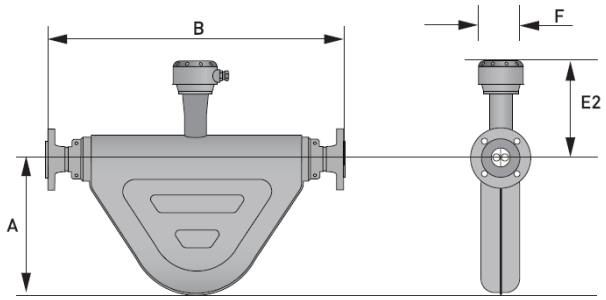

A.8. Ultrasonic Flowmeter

Manufacturer	FTI Flow Technology
Model Series	QCT_PA12
Serial Number	QCT100-2AA0
Accuracy	± 0.5 % of reading plus zero stability
Zero Stability	± 0.05 % of full scale
Repeatability	± 0.2 % over 10:1 turndown
Turndown	100
Nominal Line Sizes	2.54 cm (1 in.)
Materials of Construction	Nylon PA12
Temperature	Class A RTD
Temperature Range	(-10 to 80) °C
Max. Pressure	19 bar
Flow Rate Range	(2.65 to 265) L/min, or (0.70 to 70) gpm
Process Connection	NPT
Rating	IP 66
Power	(9 to 30) VDC
Outputs	Analog: (4 to 20) mA; Scaled frequency: (0 to 8000) Hz
Communications	Modbus RTU over EIA485
Dimensions	A = 25.4 cm (10 in.) B = 4.32 cm (1.7 in.)

C = 5.59 cm (2.2 in.)
D = 8.38 cm (3.3 in.)

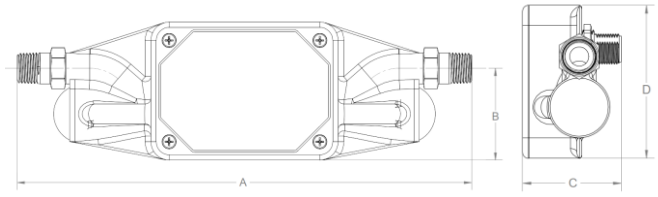

A.9. RTD

Manufacturer	OMEGA
Model Series	PR-22
Product Code	PR-22-3-100-A-1/8-0300-M12
Accuracy	IEC Class A (± 0.15 % at 0 °C)
Material	316 SS
Temperature Range	(-30 to 350) °C
Probe Length	7.62 cm (3 in.)
Probe Diameter	3.175 mm (1/8 in.)

A.10. Data Acquisition

Manufacturer	National Instruments (NI)	
Chassis	NI-9189	8-Slot, TSN-Enabled Ethernet CompactDAQ Chassis

Modules:		
Voltage Input	NI-9205	±10 V, 250 kS/s, 16-Bit, 32-Channel C Series
Voltage/Current Input	NI-9207	500 S/s, 16-Channel C Series
RTD	NI-9216	8-Channel, 400 S/s Aggregate, 0 Ω to 400 Ω, PT100 RTD C Series
Counter	NI-9361	32-Bit, 8-Channel C Series Counter Input Module
Analog Voltage Output	NI-9263	100 kS/s/ch Simultaneous, ±10 V, 4-Channel C Series
Analog Voltage Output	NI-9264	25 kS/s/ch Simultaneous, ±10 V, 16-Channel C Series
Digital Voltage Output	NI-9474	30 V, 8-Channel (Sourcing Output), 1 µs C Series
Relay Output	NI-9485	8-Channel, SSR Relay, 60 VDC/30 Vrms, 750 mA C Series